Fixed point convergence and acceleration for steady state population balance modelling of precipitation processes: application to neodymium oxalate

Cristian Camilo Ruiz Vasquez, Noureddine Lebaz, Isabelle Ramière, Sophie Lalleman, Denis Mangin, Murielle Bertrand

Fixed point convergence and acceleration for steady state population balance modelling of precipitation processes: application to neodymium oxalate

Cristian Camilo Ruiz Vasquez[1,2,*], Noureddine Lebaz[2], Isabelle Ramière[3], Denis Mangin[2], Murielle Bertrand[1]

[1] CEA, DES, ISEC, DEN, DMRC, Université Montpellier, Marcoule, France

[2] Univ Lyon, Université Claude Bernard Lyon 1, CNRS, LAGEPP UMR 5007, 43 boulevard du 11 novembre 1918, F-69100, Villeurbanne, France

[3] CEA, DEN, DEC, SESC, F- 13108 Saint-Paul Lez Durance, France

Abstract

The present work focuses on the development of a performing numerical methodology to solve the steady state Population Balance Equation (PBE) including nucleation, independent size growth and loose agglomeration as crystallization mechanisms. The methodology is based on the solution of two PBEs: one for the isolated crystallites and one describing the loose agglomerates formation. Both are solved by a discretization method and only the last one is reformulated as a fixed point problem. The algorithm solving PBE for agglomeration includes the crossed-secant algorithm as a fixed point acceleration method. The numerical PBE solution method is first validated by comparison to analytical solutions and then applied to the neodymium oxalate precipitation in order to compare to experimental results in a wide range of operating conditions. The methodology is tested under highly restrictive numerical conditions: narrow tolerances, a large amount of points in the discretization scheme and a zero vector as initial condition. The crossed-secant method demonstrates to improve the robustness of the standard fixed point iterations by ensuring the convergence of the agglomerates PBE when penalizing conditions are applied and by reducing the number of iterations otherwise. In all cases, the developed methodology predicts accurately the crystal size distribution under the experimental uncertainty in a reasonable computation time and number of iterations.

Keywords: population balance, steady state, oxalic precipitation, fixed point solution, convergence acceleration.

1. Introduction

* Corresponding author: camilo.ruiz@etu.univ-lyon1.fr

In precipitation processes, the crystal size distribution (CSD) is a decisive product property. Continuously operated well mixed precipitators present in principle poor performances in this concern [1]. For this reason, the simulation of continuous crystallizers has been the target of many modelling efforts during the last decades and remains a scientific challenge [2]. Crystallization phenomena are characterized by a strong dependence to the mixing issues: local concentrations involve local crystallization kinetics and macromixing conditions define the transport of the continuous and dispersed phases. This research work appears as a necessary step to further understanding the CSD evolution in crystallizers exhibiting complex hydrodynamics.

The evolution of the CSD in a control volume is tracked by the Population Balance Equation (PBE). The general statement at the steady state as first proposed in 1964 by Hulburt and Katz is given as [3] :

$$\frac{\partial(Gn(L))}{\partial L} + D(L) - B(L) + \sum_{i=1}^{M} \frac{F_i n_i(L)}{V} = 0 \qquad (1)$$

where L is the crystal size (m), n is the number-based density function (m^{-4}), F is the flowrate ($m^3.s^{-1}$), V is the total volume (disperse and continuous phases) (m^3),M is the total streams, G is the crystals growth rate ($m.s^{-1}$) and $B(L)$ and $D(L)$ are the birth and death terms respectively, related to the appearance and disappearance of crystals in the system (through nucleation, aggregation and breakage mechanisms). Hereafter, the CSD dependence over the size will be obviated in order to simplify equations formulation ($n = n(L)$).

The PBE is a well-known mathematical framework used to describe dispersed systems evolution. In precipitation, it is employed to determine CSD from crystallization kinetics (nucleation, growth, breakage and agglomeration) and transport phenomena. It needs to be coupled with the mass, momentum and energy balances to estimate the CSD and the supersaturation. Since several strongly coupled phenomena influence the CSD (hydrodynamics, solid dispersed particles, reaction kinetics, crystallization mechanisms, etc.), a highly nonlinear algebraic partial differential equations system needs to be solved in order to model the precipitation process. Because of the complexity of the mathematical problem, analytical solutions exist only in few cases under highly restrictive hypothesis [4]. Indeed, the numerical solution of the PBE is still an active research field [5]–[7]. Numerical solution methods can be divided into two types: those predicting some properties of the CSD (moments-based methods) and those predicting the entire CSD (discretization methods mainly) [1]. The first implies converting the original problem into ordinary differential equations via the moments transformation and the most probable crystal size distribution has to be estimated from the computed moments (inverse problem). On the other hand, discretization methods are generally known to have poor computing time performances and being highly dependent on the quantity and distribution of the nodes (discretization grid).

Most of the methods developed for the solution of the PBE aim at predicting the dispersed phase properties in a batch unit or approach the continuous process modelling as a particular case of the

transient state analysis [5], [6], [8]. The continuous steady state operation is rarely directly addressed in literature. For instance, Blandin et al. (2005) studied salicylic acid precipitation in a T-mixer modelled by a continuous well-mixed reactor followed by a plug-flow reactor operating at steady state [9]. The PBE was solved with the method of classes and the steady state in the mixing zone was given by the asymptote of the transient regime. Primary and secondary nucleations and size dependent growth were considered in the model. The steady state behaviour of polypropylene particle size was investigated by Luo et al. (2009) [10]. In this case, growth and attrition were both considered in a tubular loop reactor and the PBE was solved by a discretization method. The polymer molecular weight distribution and the particle size distribution were approached by solving the transient state population balances over an extended time scale. A Rotator Disc Contactor column operating at steady state was reported by Jaradat et al. (2010) where a multivariate PBE was coupled with hydrodynamics and applied to three chemical systems [11]. Again, the steady state PBE solution is based on asymptotic transient calculations. It is worth noticing that the dispersed phase properties obtained via transient state estimation are generally employed as initial conditions when coupled CFD-PBE steady state simulations are performed [12], [13].

When considered, steady state PBE direct calculations are often approached under highly simplifying assumptions or via underperforming algorithms. M.J. Hounslow (1990) developed a discretization method for the PBE solution in the case of steady state continuous precipitation of Nickel Ammonium Sulphate [14]. The considered PBE includes nucleation, size-dependent growth and aggregation but computing speed drastically decreases with the number of nodes used in the discretization scheme. Nicmanis et al. (1998) developed a collocation-Galerkin based method to solve the steady state PBE accounting for nucleation, growth, agglomeration and breakage mechanisms [15]. In this case, the system of equations was solved by an iterative process and validated via numerical case studies and analytical solutions. The numerical performance of the traditional discretization method is improved but the selection of interpolation functions and collocation points remains a mathematical constraint. Semlali et al. (2001) solved the steady state PBE applied to a sugar continuous crystallizer taking into account a compartmental-based mixing model [16]. Since only nucleation and growth were included as crystallization mechanisms, PBE solution was possible through analytical solutions. More recently, Alzyod et al. (2016) simulated a liquid-liquid extraction column where the steady state properties of the droplet size distribution are predicted thanks to a moments-based method [17]. Even if computational performances were found to be satisfactory, only mean droplet size and liquid phase compositions are predicted. Detailed information on the droplet size distribution are not reachable using this solution methodology.

The PBE concerned in this study considers three crystallization phenomena, namely nucleation, growth and loose agglomeration. The last one is a particular case of agglomerates formation: the developed surface of crystals created by nucleation and growth is the same whether the agglomeration phenomenon takes place or not. The study of loose agglomerates is hardly aimed in literature. The formulation of the PBE in such case results in the separation of agglomeration from

nucleation and growth mechanisms. Consequently, two successive PBEs have to be solved: one accounting for the isolated crystals (crystallites) and one accounting for the agglomerates [18].

The purpose of this study is to develop a PBE-based model for a Mixed Suspension Mixed Product Removal (MSMPR) precipitator including nucleation, growth and loose agglomeration as crystallization mechanisms. The novelty lies in the numerical solution methodology based on the solution of two steady state PBEs: one considering the nucleation and growth phenomena and one regarding only the loose agglomeration. The solution of the agglomeration PBE is performed by a fixed point method and includes the crossed secant method as a fixed point acceleration algorithm. This methodology aims at predicting the CSD leaving a MSMPR with no assumption on the feed streams in a reasonable time calculation for further coupling with a multicompartment model and/or CFD simulations.

In order to test this numerical strategy, the oxalic precipitation (equation (2)) is considered as application case. In the nuclear industry, this reaction is widely used as the main conversion and purification stage leading to the production of an actinide riche powder from a multicomponent solution. Due to economic and environmental considerations, the study of actinides precipitation is traditionally approached by the investigation of harmless elements such as lanthanides [18], [19]. Hence, the neodymium oxalate precipitation in a MSMPR precipitator is investigated in this study. The reaction kinetics is considered fast enough to neglect its influence on the entire process:

$$2Nd(NO_3)_3 + 3H_2C_2O_4 \xrightarrow{H_2O} Nd_2(C_2O_4)_3 \cdot 10H_2O + 6HNO_3 \quad (2)$$

The structure of this paper is as follows: In Section 2, the PBEs are formulated and the corresponding numerical solution methods are described. The fixed point problem solving the agglomeration PBE at steady state is established. A suitable fixed point acceleration method is then introduced in order to improve the performance of the solution algorithm but also to ensure its robustness, especially when standard fixed point iterations would diverge. In Section 3, simulation results are first validated by comparison to analytical solutions and then tested against a range of experimental data. Finally, some concluding remarks and perspectives are pointed out.

2. Modelling strategy

During continuous precipitation, the CSD and continuous phase composition are the target variables to be predicted since they determine the quality of the produced powder and the recovery of the desired compound. CSD is detailed by the PBE as described in the last section. Furthermore, liquid phase concentrations need mass balances to be evaluated. Thus, the system of equations describing the precipitator includes both mass balances on the continuous and dispersed phases and the PBE.

One may note that crystallization kinetics vary with species concentrations in the continuous phase via the supersaturation. In parallel, the concentrations of the reagents remaining in the liquid phase are

determined by the extent of the chemical reaction and further by the amount of solid accounted in the mass balances.

2.1. PBE solution

Equation (1) assembles all the physicochemical processes modifying the CSD, namely the transport phenomena and the crystallization mechanisms. The precipitator considered in this study has several inlet flows $(F_i)_{i=1}^{M-1}$ that may contain particles in suspension and one single exit flow (F_M). The mean residence time is thus defined as $\tau = \frac{V}{F_{out}}$ and the outgoing flow rate as $\sum_{i=1}^{M-1} F_i = F_{out}$. Assuming an MSMPR precipitator, operating at steady state, with nucleation, size independent growth and agglomeration, the PBE can be written as:

$$G\frac{\partial n}{\partial L} + \frac{n_{out}(L) - \frac{\sum_{i=1}^{M-1} F_i\, n_i}{F_{out}}}{\tau} = R_N \cdot \delta(L - L^*) + h \tag{3}$$

with

$$h = \frac{L^2}{2}\int_0^L \frac{\beta\left((L^3-\lambda^3)^{1/3}, \lambda\right) n_{out}\left((L^3-\lambda^3)^{1/3}\right) n_{out}(\lambda, t)\, d\lambda}{(L^3-\lambda^3)^{2/3}} - n\int_0^\infty \beta(L,\lambda) n_{out}(\lambda) d\lambda \tag{4}$$

where L and λ represent the particle size (m), δ is the Dirac delta function, L^* the nuclei size (m), R_N ($m^{-3}.s^{-1}$) the nucleation rate, β represents the agglomeration kernel ($m^3.s^{-1}$), and n_{out} the density associated to the output stream. The term h accounts for the particles appearing and disappearing by agglomeration, $B(L)$ and $D(L)$ respectively. Note that no assumption is made regarding the feed streams, therefore the PBE model solved in this work deals with single or multiple feedings whether they include crystals in suspension or not.

Equation (3) is a highly nonlinear integro-differential equation. In this work, the steady state PBE accounting for nucleation, growth and agglomeration is solved by a discretization method. Neodymium oxalate crystals have been identified as loose (open) agglomerates according to microscopic observations: the surface of crystals in contact with the surrounding solution is the same at any stage of the agglomeration process [18]. Thus, the growth mechanism takes place at the surface of every elementary particle forming an agglomerate and is considered as non-affected by the internal diffusion. In other words, growth and agglomeration can be modelled as independent phenomena since the first affects the crystallites size whereas the second modifies the agglomerates size. Considering this, the steady state PBE solution is performed by describing the whole precipitation process through two distinct PBEs solved successively. The first one accounts for nucleation and growth mechanisms and the second one considers the crystallites agglomeration only, using the CSD obtained as a result of the first PBE. Previously, a similar methodology was implemented in order to determine the neodymium oxalate agglomeration kernel [18].

2.1.1. PBE for nucleation and growth mechanisms

The steady state PBE for a MSMPR undergoing only nucleation and size independent growth phenomena, leading to the crystallites size distribution function $n_{out,1}$, is written as:

$$G\frac{dn_{out,1}}{dL}+\frac{n_{out,1}}{\tau}-\frac{\frac{\sum_{i=1}^{M-1}F_i\,n_i}{F_{out}}}{\tau}=R_N\cdot\delta(L-L^*) \tag{5}$$

Assuming that crystals born at zero size, and that $n_{out,1}(L=0)=\ n_{out,1}^0$, equation (5) can be rewritten as:

$$G\frac{dn_{out,1}}{dL}+\frac{n_{out,1}}{\tau}-\frac{\frac{\sum_{i=1}^{M-1}F_i\,n_i}{F_{out}}}{\tau}=0 \tag{6}$$

with the boundary condition:

$$n_{out,1}^0=\frac{R_N}{G} \tag{7}$$

Equation (6) is an ordinary differential equation which can be easily solved when the inlet population (n_i) and the nucleation and growth rates are known. The population fed to the reactor is set as an input variable, the nucleation and growth rates depend on the species concentration in the solution via the supersaturation. The concentration of the precipitating compound and the CSD flowing out the precipitator have also to satisfy the mass balance, both are initially unknown. The nucleation and growth PBE is computed over the discretized size vector $(L_k)_{k=1}^K$ by numerical integration (K is defined as the total number of nodes in the discretization grid). It is solved simultaneously with the mass balance by a minimisation iterative gradient-based method (Sequential Quadratic Programming method). The objective function aims to converge to a concentration in solution satisfying both the PBE and the mass balance. The stopping criterion is determined by the relative difference between the concentration calculated at two successive iterations.

2.1.2. PBE for agglomeration

The second steady state PBE concerns only the agglomeration phenomenon. It is expressed as:

$$\frac{n_{out,2}\ -\frac{\sum_{i=1}^{M-1}F_{i,2}\,n_{i,2}}{F_{out,2}}}{\tau}=\frac{L^2}{2}\int_0^L\frac{\beta\left((L^3-\lambda^3)^{1/3},\lambda\right)n_{out,2}\left((L^3-\lambda^3)^{1/3}\right)n(\lambda)\,d\lambda}{(L^3-\lambda^3)^{2/3}}-\ n_{out,2}(L)\int_0^\infty\beta(L,\lambda)\,n_{out,2}(\lambda)d\lambda \tag{8}$$

From a theoretical point of view, the agglomeration process can be divided into two steps: particle collision and bonds consolidation. The loose agglomerates assumption implies that the amount of matter needed to bond crystallites does not modify the free surface of the initial particles. Thus, the amount of precipitating compound used to build these bonds can be neglected from the mass balance. Consequently, the solution of the PBE for agglomerates requires the supersaturation, the composition

of the output stream and the crystallites CSD as input information. Equation (8) is solved by the fixed pivot technique proposed by Kumar and Ramkrishna (1996) [20]. The number-based density function (n) is substituted by the total number of particles (N), defined by the integration of (n) over a discrete size interval $[b_k, b_{k+1}]$:

$$N(L_k) = \int_{b_k}^{b_{k+1}} n(L)\, dL \tag{9}$$

with L_k, $k = 1, \dots, K$ the representative size for the k^{th} size range obtained by discretization of the size domain $[L_{min}, L_{max}]$ in K elements and b_k and b_{k+1} the lower and upper boundaries for the k^{th} size range respectively. The right-hand side of equation (8) defines the agglomeration rate r_{Ag} ($m^{-4}\, s^{-1}$):

$$r_{Ag}(L_k) = \frac{L^2}{2}\int_0^L \frac{\beta\left((L^3-\lambda^3)^{1/3}, \lambda\right) n_{out,2}\left((L^3-\lambda^3)^{1/3}\right) n(\lambda)\, d\lambda}{(L^3-\lambda^3)^{2/3}} - n_{out,2}(L)\int_0^\infty \beta(L,\lambda)\, n_{out,2}(\lambda) d\lambda \tag{10}$$

The discretized agglomeration rate, still called $r_{Ag}(L_k)$, is given as proposed by Kumar and Ramkrishna (1996) [20]:

$$r_{Ag}(L_k) = \sum_{\substack{p,q=1 \\ p \geq q}}^{p=K} \left[\left(1 - \tfrac{1}{2}\delta_{p,q}\right) \eta\, \beta(L_p, L_q)\; N_{2,out}(L_p) N_M(L_q)\; \right] - N_{2,out}(L_k) \sum_{r=1}^{K} \beta(L_k, L_r)\; N_{2,out}(L_r) \tag{11}$$

under the following conditions:

$$L = \left(L_p^3 + L_q^3\right)^{1/3}, \;\; L_{k-1} \leq L \leq L_{k+1} \tag{12}$$

$$\eta = \begin{cases} \dfrac{L_{k+1}^3 - L^3}{L_{k+1}^3 - L_i^3}, & L_k \leq L \leq L_{k+1} \\ \dfrac{L^3 - L_{k-1}^3}{L_k^3 - L_{k-1}^3}, & L_{k-1} \leq L \leq L_k \end{cases} \tag{13}$$

where $\delta_{p,q}$ is defined as the Kronecker delta function, $N_{2,out}(L_k)$ represents the total number of particles in the k^{th} size range (class). The weight coefficient η ensures the conservation of two properties (number and mass). In the agglomeration problem, the unknown variable is defined as $N_{2,out}(L_k)_{k=1}^K = \boldsymbol{N}$ which refers to the vector resulting from the discretization of the number-based CSD over the crystal size $(L_k)_{k=1}^K$. By substituting equation (11) in equation (8) and by defining the inlet population (before agglomeration process) as $\boldsymbol{N}_{in} = N_{in}(L_k)_{k=1}^K = \frac{\sum_{i=1}^{M-1} F_i\, N_i(L_k)_{k=1}^K}{F_{out}}$, equation (11) leads to a system of K equations:

$$\boldsymbol{N} = \boldsymbol{f}(\boldsymbol{N}) = \boldsymbol{N}_{in} + \tau\, \boldsymbol{r_{Ag}}(\boldsymbol{N}) \tag{14}$$

where the function $f(\boldsymbol{N})$ represents the agglomeration PBE. The simplest way to solve the fixed point problem $\boldsymbol{N} = f(\boldsymbol{N})$ in equation (14) is to use fixed point iterations (or Picard iterations). Hence the j^{th} iteration is defined as:

$$\boldsymbol{N}^j = \boldsymbol{f}(\boldsymbol{N}^{j-1}) = \boldsymbol{N}_{in} + \tau\, \boldsymbol{r_{Ag}}(\boldsymbol{N}^{j-1}) \tag{15}$$

Fixed point iterates can be seen as pseudo-transient solutions (pseudo-time steps) before reaching the steady state. However, the convergence of the fixed point sequence strongly depends on the properties of the fixed point function $\boldsymbol{f}$ (namely its spectral radius in the neighbourhood of the fixed point solution), which are generally *a priori* unknown. Hence, the convergence of the fixed point iterations (equation (15)) is not guaranteed.

In most precipitation processes, the objective variable $\boldsymbol{N}$ varies over several orders of magnitude (between 0 and 10^{25} in the case of the neodymium oxalate). For this reason, the following mixed convergence criterion is used as in [21]:

$$\left| f_k(\boldsymbol{N}^j) - N_k^j \right| < \varepsilon_r \left| N_k^j \right| + \varepsilon_a, \ \forall k \tag{16}$$

where the index k refers to the k^{th} component of the vector. Thus the fixed point convergence is reached when the difference between two successive iterates (left-hand side term) is less than the total of the tolerances (right-hand side terms). The right-hand side terms include two tolerance constants: the relative tolerance ε_r and the absolute tolerance ε_a .This convergence criterion turns automatically from a relative error to an absolute error when $\left|N_k^j\right|$ becomes small. Hence it enables to deal in a unique criterion with high values of N components (for which the relative precision is recommended) and small values of N components (where absolute tolerance is required).

In practice, it is common to represent Equation (16) as a boolean:

$$\max_{(\mathbf{k})} \left(\left| f_k(\boldsymbol{N}^j) - N_k^j \right| - \varepsilon_r \left| N_k^j \right| - \varepsilon_a \right) < 0 \tag{17}$$

It is worth noticing that when the peak region (high values of N components) is of interest, the absolute tolerance could remain relatively high, in order to focus on the convergence of the solution in the peak region (with a relative error).

2.2. Fixed point convergence acceleration methods

Fixed point iterations are a powerful tool to solve highly non-linear problems, since the algorithm can be applied to any objective function and no information about its derivative is required to implement the method. Nevertheless, in case of convergence, they are often characterized by a slow first order convergence which can become time consuming [22], [23]. As the PBE concerned in this paper is a strongly non-linear and high dimensionality problem, acceleration methods are considered to improve both algorithm performances and robustness. Indeed, as shown in section 3, the fixed point algorithm applied to the agglomeration problem may result in a divergent sequence. Acceleration algorithms are then introduced to ensure fixed point convergence in such cases and to reduce the calculation time (number of iterations) when standard fixed point iterations converge.

In equation (15), the standard iterates $\boldsymbol{N}^j$ are defined by a recurrence relation and can be treated as a series. Then, classical sequence acceleration principles can be applied. In numerical analysis, two types of convergence acceleration methods are commonly studied: the static and the dynamic acceleration procedures. The second is commonly used in practice as it consists in substituting the current fixed point value ($\boldsymbol{f}(\boldsymbol{N}^j)$), by an accelerated iterate which improves the convergence rate [24]. Many expressions for the accelerated sequence have been proposed in the literature depending on the characteristics of the initial mathematical problem. In general, it is defined as a function of the previous accelerated and standard iterates [23]. Ramiere et al. (2015) proposed a general framework to obtain accelerated sequence expressions from a nonlinear hybrid acceleration procedure applied to

vector-based fixed point problems [25]. In this research work, three acceleration methods were tested to solve the PBE.

The first one is the classical scalar secant method applied independently on each component of the unknown vector $\boldsymbol{N}$. For a scalar fixed point problem, $x = f(x)$, $x \in R$, this method can be geometrically interpreted as finding the intersection of the line passing through the two points $(x^{j-1}, f(x^{j-1}))$ and $(x^j, f(x^j))$, and the first bisector of the axes $(y = x)$. The abscissa of this intersection point defines the new iterate x^{j+1}. It is hence mathematically defined as (see for example [26]):

$$x^{j+1} = f(x^j) - \frac{\left(f(x^j) - f(x^{j-1})\right)(f(x^j) - x^j)}{(f(x^j) - x^j) - (f(x^{j-1}) - x^{j-1})} \tag{18}$$

In this work, Equation (18) is applied independently on each scalar $N_k, k = 1, \dots K$:

$$N_k^{j+1} = N_k^j - \frac{\left(N_k^j - N_k^{j-1}\right)\left(f_k(\boldsymbol{N}^j) - N_k^j\right)}{\left(f_k(\boldsymbol{N}^j) - N_k^j\right) - \left(f_k(\boldsymbol{N}^{j-1}) - N_k^{j-1}\right)} \quad , \forall k \tag{19}$$

The second and third acceleration methods tested in this work can be obtained by the application of the secant principle when considering a vector fixed point problem. As each component N_k does not define a scalar fixed point problem, vector sequence acceleration should be applied on the whole vector $\boldsymbol{N}$. The vector secant methods can be directly obtained by considering the (non unique) definition of the inverse of a vector:

$$\boldsymbol{X}^{-1} = \frac{\boldsymbol{X}}{\|\boldsymbol{X}\|^2}, \quad \boldsymbol{X} \in R^K \tag{20}$$

where ||.|| represents a given norm, generally the Euclidean norm. Considering equations (18) and (20), two vector secant methods can be derived based on the two possible dot products arising in the numerator. In Ramière et al (2015), it has been proven that these vector secants can be seen as a minimization process on fixed point residuals [25]. For the sake of clarity, the following residual notation is introduced: $\Delta\boldsymbol{N}^j = \boldsymbol{f}(\boldsymbol{N}^j) - \boldsymbol{N}^j$. The two vector-based secant acceleration methods obtained write:

- The alternate secant method:

$$\boldsymbol{N}^{j+1} = \boldsymbol{f}(\boldsymbol{N}^j) - \frac{(\Delta\boldsymbol{N}^j - \Delta\boldsymbol{N}^{j-1}) \cdot \Delta\boldsymbol{N}^j}{\|\Delta\boldsymbol{N}^j - \Delta\boldsymbol{N}^{j-1}\|^2} \left(\boldsymbol{f}(\boldsymbol{N}^j) - \boldsymbol{f}(\boldsymbol{N}^{j-1})\right) \tag{21}$$

- The crossed secant method:

$$\boldsymbol{N}^{j+1} = \boldsymbol{f}(\boldsymbol{N}^j) - \frac{\left(\boldsymbol{f}(\boldsymbol{N}^j) - \boldsymbol{f}(\boldsymbol{N}^{j-1})\right) \cdot (\Delta\boldsymbol{N}^j - \Delta\boldsymbol{N}^{j-1})}{\|\Delta\boldsymbol{N}^j - \Delta\boldsymbol{N}^{j-1}\|^2} \Delta\boldsymbol{N}^j \tag{22}$$

The K-dimensional scalar secant approach (Equation (19)) prevented the divergence of the fixed point iterations but did not reduce significantly the number of iterations. The alternate secant method did not improve the fixed point iterations convergence at all, Finally, the crossed secant method was selected

to solve agglomerates PBE as it presented really advantageous properties especially in case of divergence of the standard fixed point iterations (see Appendix 1).

As the fixed point sequence and the accelerated one are not mathematically constrained to fit the same limit [25], the convergence criterion defined in equation (17) must still focus on the standard fixed point residual $(\boldsymbol{f}(\boldsymbol{N}^j) - \boldsymbol{N}^j)$ to guarantee the solution of equation (14).

3. Results and discussion

3.1. Validation through analytical solutions

As described previously, the methodology developed in this work implies the formulation of two different population balances to describe precipitation process. As a first step, analytical solutions were employed to validate the numerical approach developed to solve each PBE separately. All the simulations were performed using the same standard personal computer.

3.1.1. PBE for nucleation and growth mechanisms in a cascade of two precipitators

Equation (6) may be solved analytically when the reactor is fed with a single flow of clear solution ($n_1 = 0$). In such case, the CSD flowing out the reactor is determined by [27]:

$$n_{out,1,1} = n^0_{out,1,1}\, exp\left(\frac{-L}{G\,\tau}\right) \tag{23}$$

In order to test the methodology when the precipitator is fed with a suspension, the CSD flowing through a cascade of two precipitators is studied. Thus the CSD at the output of the second precipitator ($n_{\mathrm{out},1,2}$) is determined analytically as [28]:

$$n_{\mathrm{out},1,2} = n^0_{\mathrm{out},1,2}\, exp\left(\frac{-L}{G_2\,\tau_2}\right) + \frac{F_{\mathrm{out},1}}{F_{\mathrm{out},2}} n^0_{\mathrm{out},1,1} \left[\frac{G_1\,\tau_1}{G_1\,\tau_1 - G_2\,\tau_2}\right]\left[exp\left(\frac{-L}{G_1\,\tau_1}\right) - exp\left(\frac{-L}{G_2\,\tau_2}\right)\right] \tag{24}$$

Both analytical solutions (equations (23) and (24)) are compared to the CSD obtained by the numerical method detailed in section 2.1.1 (Figure 1). Simulation points are obtained with a discretization grid containing 1500 logarithmically distributed values between 10^{-11} and 10^{-4} m for the integration rule. The relative tolerance in the mass balances is set to 10^{-6} and the calculation time is less than 10 seconds for both precipitators on an Intel Core i7 machine (1.90 GHz/2.11 GHz) with 32 Go of RAM. Figure 1 shows that the numerical and analytical results are identical with a relative difference less than 10^{-4}.

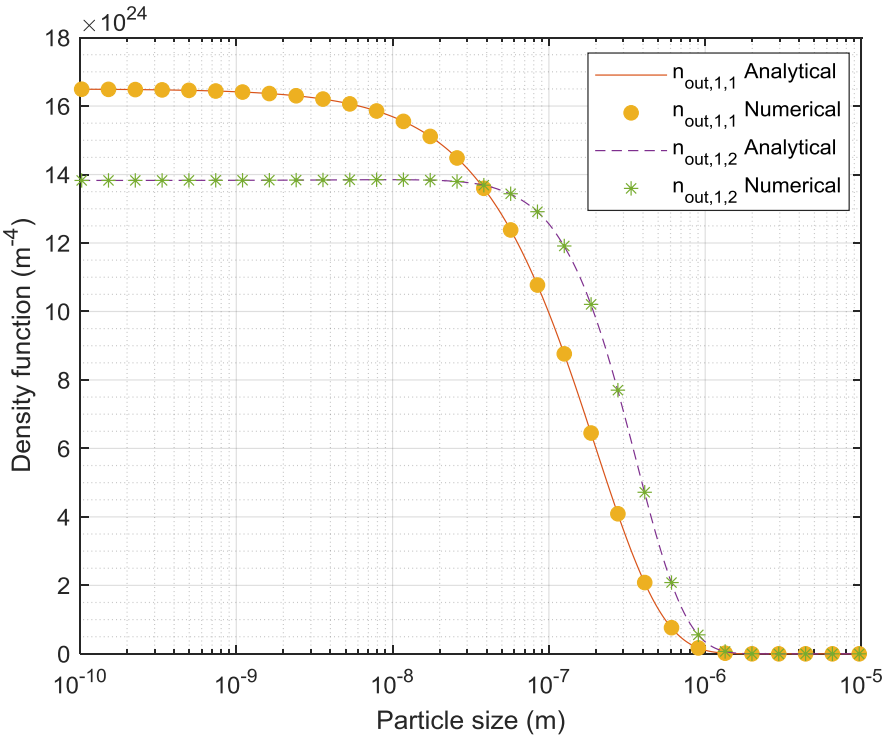

Figure 1. Comparison between the numerical solution methodology and the analytical solutions: output CSD for two reactors in series considering nucleation and size-independent growth.

3.1.2. PBE for agglomeration with size independent kernel

Steady state agglomeration problems can be solved analytically only when the agglomeration kernel is independent of the crystal size and the inlet population follows a normal distribution. In such case, Hounslow (1990) developed an analytical solution based on the crystal volume as internal coordinate and dimensionless variables [14]:

$$J(x) = \frac{I_0\left[\frac{-t'x}{1+2\,t'}\right] + I_1\left[\frac{-t'x}{1+2\,t'}\right]}{exp\left(\frac{(1+t')x}{1+2\,t'}\right)\sqrt{1+2\,t'}} \tag{25}$$

where

$$t' = N_0\,\beta\,\tau\ , \quad J(x) = n_{out,2}(v)\frac{v_0}{N_0}\ , \quad x = \frac{v}{v_0} \tag{26}$$

v represents the crystal volume, I_0 and I_1 are the modified Bessel functions of the first kind, of order zero and one respectively, t' the characteristic time of the agglomeration process, v_0 and N_0 are characteristics of the inlet population, namely the mean crystal volume and the total amount of particles.

Figure 2 a) presents a comparison between the analytical solution given in equation (25) and the numerical solution obtained through the accelerated method described in section 2.2 in terms of the total number of particles. Three values of the t' parameter are examined in order to verify results coherence and algorithm robustness. In every case, 200 logarithmically distributed points are used to

define the discretization grid. The numerical and the analytical solutions match with a relative tolerance lower than 10^{-4}.

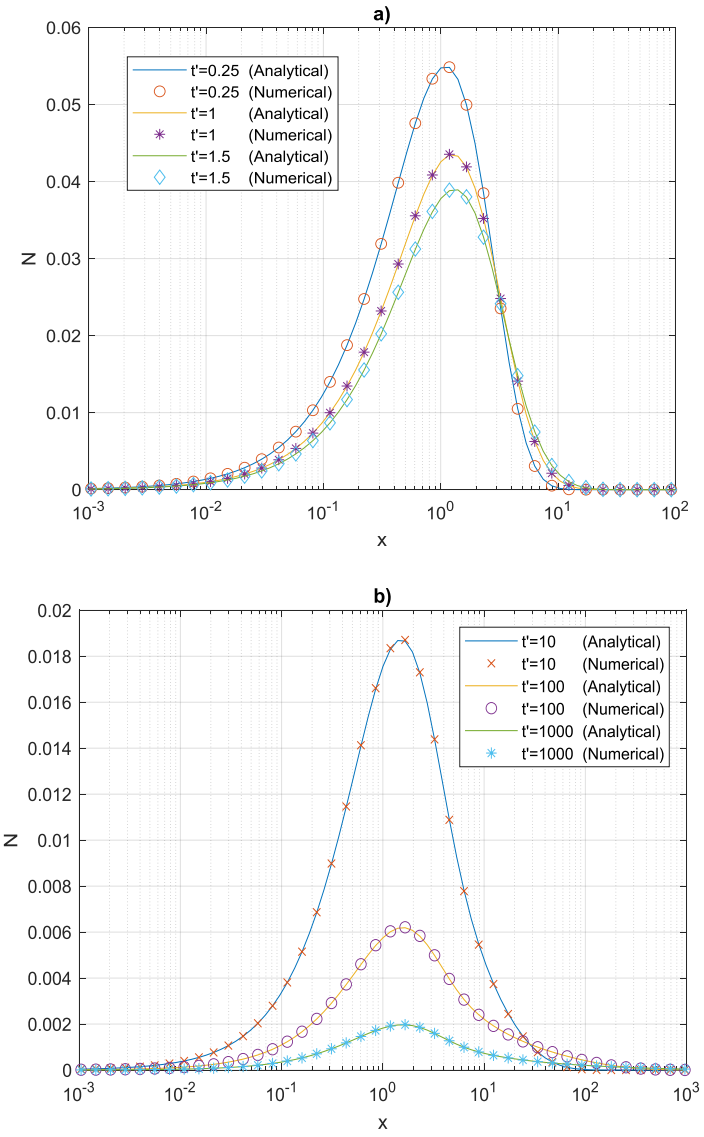

Figure 2. Comparison between the CSD obtained by the developed numerical methodology and the analytical solution for the agglomeration problem.

In the context of a multicompartmental model, t' is expected to take values over 100. Additionally, CSD estimation has to be performed between the nuclei size (about 10^{-9} m) and the agglomerates maximum size (about 10^{-4} m), conditioning the number of intervals in the discretization to be large enough to track the smaller particles and the mean size region simultaneously. Figure 2 b) presents the comparison between the numerical and the analytical solutions for t' varying between 10 and 1000. Again, 200 logarithmically distributed points are used to define the discretization grid. With such values of t', the accelerated algorithm enables the agglomerates PBE to converge when standard fixed point iterations diverge.

Appendix 1 summarizes the main results obtained with the fixed point algorithm and the tested acceleration methods for two different values of t' (1 and 10^3 respectively), both N_0 and β were chosen

to match the order of magnitude observed in the case of the precipitation of neodymium oxalate. The crossed secant method clearly appears to be the most performant method to accelerate fixed point iteration convergence but also to guarantee sequence convergence.

It is worth underlying that a relevant initialization vector ($\boldsymbol{N}^0$) is also required to obtain the best performances. The determination of an optimal initial vector could be a hard mathematical task and return to the solution of the problem itself. Three numerical choices (null initialization, based only on crystallites CSD and based on both the crystallites CSD and the agglomeration dimensionless time (t')) have been tested (see Appendix 1). A null initialization vector ($\boldsymbol{N}^0 = 0$) appears to be a simple but robust choice.

Appendix 2, in which the acceleration algorithm is applied to a theoretical case ($\beta = 1$ and $N_0 = 1$), shows that the efficiency (in terms of number of iterations) of the standard fixed point algorithm and the crossed secant method does not depend on the quantity of points used to discretize the internal coordinate (crystals size or volume), except for large agglomeration characteristic times. However, as expected the calculation time increases with the number of unknowns. One may observe that the number of iterations required to converge increases with the agglomeration dimensionless time (t'). Actually, divergence of standard fixed point iterations is observed for $t' > 1.5$. Also, the number of iterations to converge depends on the values of τ, β and N_0. For this reason, a different number of iterations is observed when $t' = 1$ on Appendix 1 and Appendix 2.

3.2. Application case: oxalate neodymium precipitation

3.2.1. Case study

Lalleman et al. (2012) presented results for neodymium oxalate precipitation [18]. The experiments were carried out in a stirred tank reactor provided with a heating jacket and four stainless steel baffles. Mixing was performed by a stainless-steel turbine equipped with four 45° pitched blades.

Oxalic precipitation was achieved by mixing an aqueous solution of neodymium nitrate with an aqueous solution of oxalic acid. For the purpose of this study, the reagents concentrations in the reactor obey to the stoichiometric ratio of equation (2) and the neodymium oxalate was the only compound found in the outgoing crystals. Mean residence time is about 1 minute and the steady state is typically reached after 15 minutes. Slurry samples were taken from the output stream and analysed with a laser diffraction granulometer in order to obtain the steady state CSD in the output flow.

The nucleation rate R_N for the neodymium oxalate is expressed as [19]:

$$R_N = 3.2 * 10^{31}\ exp\left(-\frac{66700}{R\,T}\right)\ exp\left(-\frac{187}{(\ln S)^2}\right) \tag{27}$$

with T the temperature (K) and S the driving force, namely the relative supersaturation defined as:

$$S = \gamma_{\pm}\left(\frac{C_{Nd}^{2} C_{C_2O_4}^{3}}{P_s}\right)^{0.2} \tag{28}$$

where the activity coefficient $\gamma_{\pm}$ is computed from the Bromley correlation [29] with the individual contribution values proposed by Lalleman et al. (2012) for the neodymium electrolytes [30], C is the molar concentration (mol.m^{-3}) and P_s the solubility product (mol^{5}.m^{-15}).

In the case of the oxalic precipitation of neodymium, the growth rate was found to be independent of the crystal size and integration-controlled [19]:

$$G = 2.9 * 10^{-6} \exp\left(-\frac{14000}{R\,T}\right) (P_s)^{1/5} (S-1) \tag{29}$$

Similarly, the neodymium oxalate agglomeration process was found to be independent of the crystal size [18], the agglomeration kernel is expressed as:

$$\beta = 2.55 * 10^{-7}\, I^{-0.7}(S-1)\dot{\gamma}^{-0.24} \exp\left(-\frac{40900}{R\,T}\right) \tag{30}$$

where $\dot{\gamma}$ is the shear rate (s^{-1}) and I the ionic force of the solution (mol.m^{-3}).

3.2.2. PBE modelling

In a first time, the developed methodology is tested against a reference experience (Experiment 1 in Table 1)Table 1. Figure 3 presents the behaviour of the agglomeration PBE convergence criterion (equation (17)) over the number of iterations when the developed methodology is applied to a MSMPR precipitator including nucleation, growth and agglomeration mechanisms. The discretization grid contains 1500 logarithmically distributed points between 10^{-11} m and 10^{-3} m.

Standard fixed point iterations (Figure 3 (a)) do not succeed to converge due to the value of the dimensionless agglomeration time. In contrast, the crossed-secant accelerated fixed point achieves the agglomerates CSD prediction after 237 iterations (Figure 3 (b)). Simulation time for the case study is about 80 seconds on an Intel Core i7 machine (1.90 GHz/ 2.11 GHz) with 32 Go of RAM, the relative tolerance (ε_r) is fixed to 10^{-2} while the absolute tolerance is defined as a function of the crystallites CSD: $\varepsilon_a = \frac{\max_{(k)}(\boldsymbol{N}_{in})}{10^{6}}$. Following the previous study (see also Appendix 1), the initial vector for the fixed point algorithm solving the agglomeration PBE is set to zero.

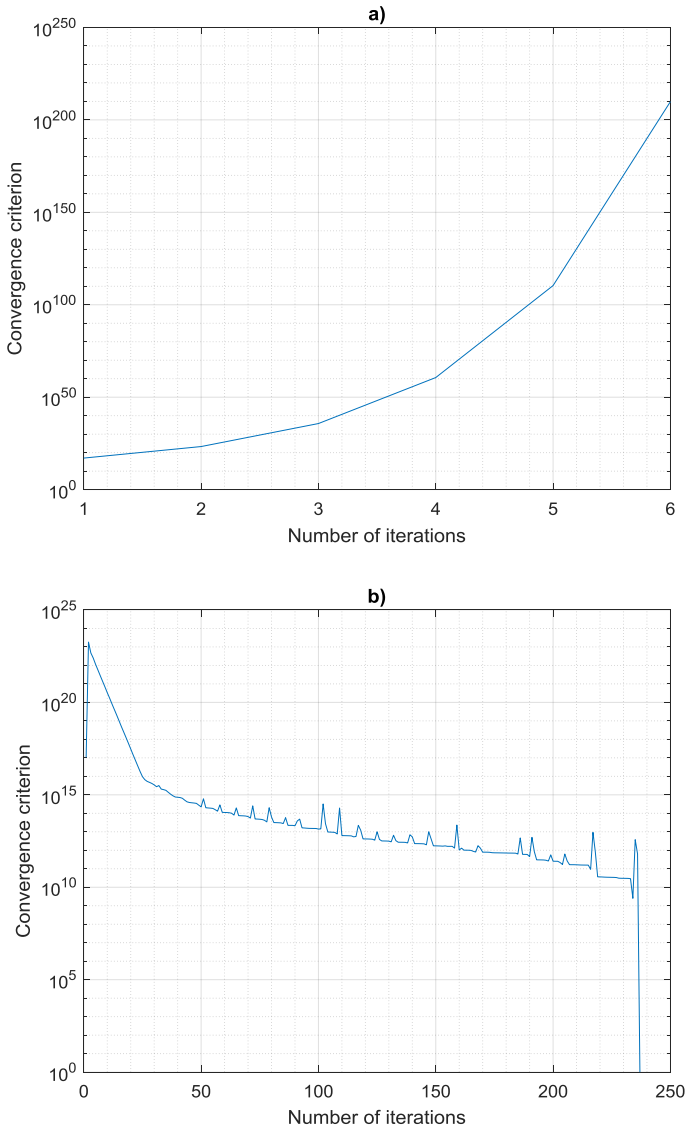

Figure 3. Convergence criterion evolution in the case of a MSMPR modelling including nucleation, size-independent growth and loose agglomeration with (a) standard fixed point algorithm b) accelerated fixed point algorithm.

Crystal mean size is correctly predicted under the experimental incertitude (Figure 4 a). The same observation is made concerning the moments, only the 0^{th} order moment is slightly over predicted by 5% (Figure 4 c)). In contrast, a broader difference is observed when the entire CSD is examined (Figure 4 b)). The gap between the simulated and the experimental CSD arises from the uncertainty associated to the crystallization kinetics. Firstly, nucleation kinetics typically predicts the quantity of elementary crystals over one order of magnitude. Secondly, the methodology employed to determine the neodymium oxalate agglomeration kernel includes the solution of the PBE by the moments method [18]. Such numerical treatment ensures a precise calculation of the moments but generates errors in CSD prediction due to the lack of information about the entire distribution.

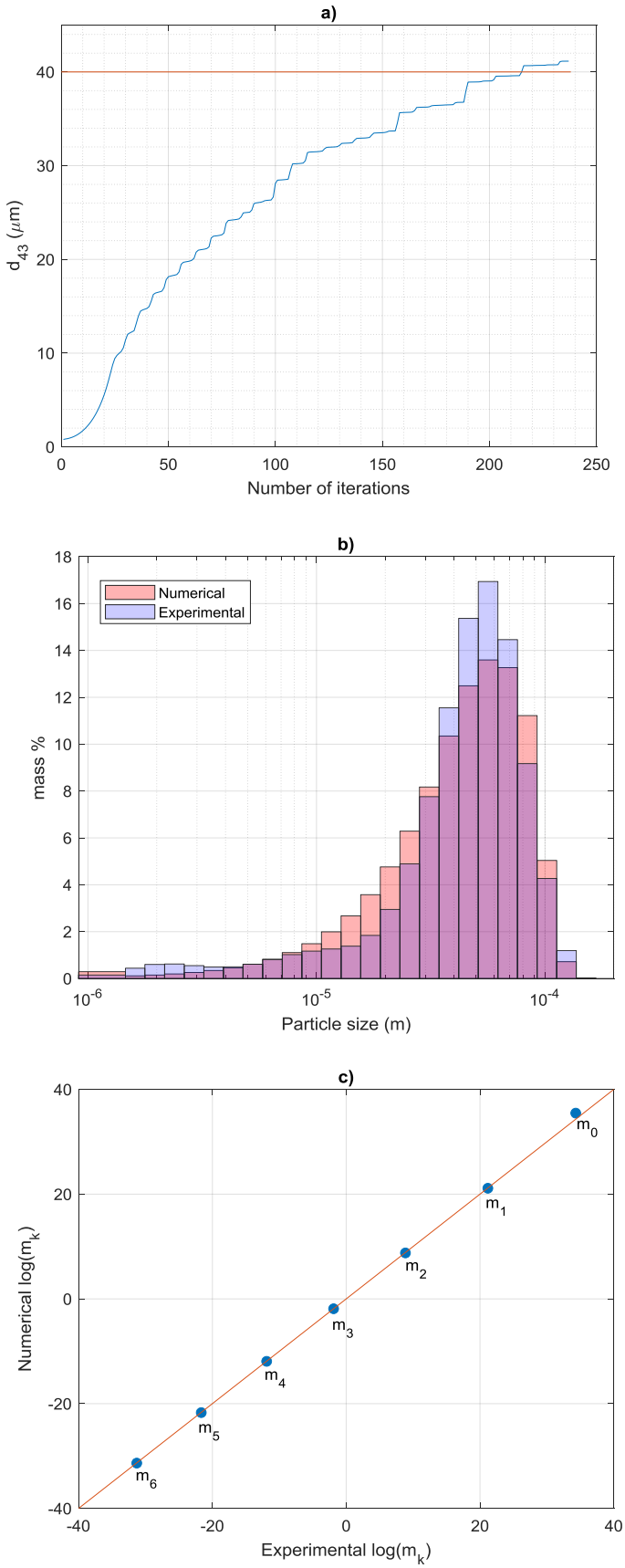

Figure 4. Experimental and simulation results in the case of a MSMPR including nucleation, size-independent growth and loose agglomeration: a) Mean crystal size prediction over the number of iterations b) Mass-based CSD and c) CSD moments

3.2.3. Sensitivity analysis

The developed algorithm is tested under several operating conditions. Experimental details and resulting mean sizes are presented in Table 1. Variation of three operating conditions are tested: the temperature, the shear rate via the stirring rate and the total neodymium concentration via the inlet stream concentration. Mean residence time, reagents proportions, and other experimental parameters remain the same as in the reference case (Experiment 1).

Table 1. Experimental conditions, mean crystal size and numerical performances for the simulation of a continuous crystallizer including nucleation, size-independent growth and loose agglomeration.

Experiment	$[Nd]_0$ (mol m^{-3})	T (K)	Υ (s^{-1})	Experimental d_{43} (µm)	Simulated d_{43} (µm)	Number of iterations (Agglomeration PBE)	Calculation time (s)
1	62.0	293.15	362	45	43	237	76
2	201.7	293.15	362	53	53	272	92
3	284.9	293.15	362	59	56	274	83
4	142.2	293.15	665	48	47	319	97
5	142.2	293.15	1024	41	46	250	84
6	144.7	303.15	362	55	53	303	92
7	144.7	313.15	362	54	57	317	91
8	144.7	323.15	362	60	60	306	89

Experimental and numerical volume-based mean sizes (d_{43}) obtained for the experiments described in Table 1 are plotted in Figure 5. Calculation time is lower than 100 seconds for all the examined cases. Also, the number of iterations is about 300 for the worst case and no direct dependency is observed with any of the studied variables. The proposed algorithm seems to be robust.

From **~~Erreur ! Source du renvoi introuvable.~~** Table 1, the mean size of the examined distributions increases with the concentration of Nd and with the temperature. In both cases, the crystallization kinetics are systematically strengthened: a higher concentration implies a higher supersaturation from equations (27), (29) and (30). Similarly, the crystallization phenomena occur faster when the temperature is raised. In both cases, larger particles are expected. In contrast, it is not possible to establish a direct link between the shear rate and the mean crystal size, the latter could increase or decrease due to the compromise between mixing performance and mechanical resistance of the crystals. For this reason, a direct tendency is less observable when experiments 4 and 5 are considered. In all the cases the mean size is well predicted considering the experimental uncertainty and the evolution over the examined variables.

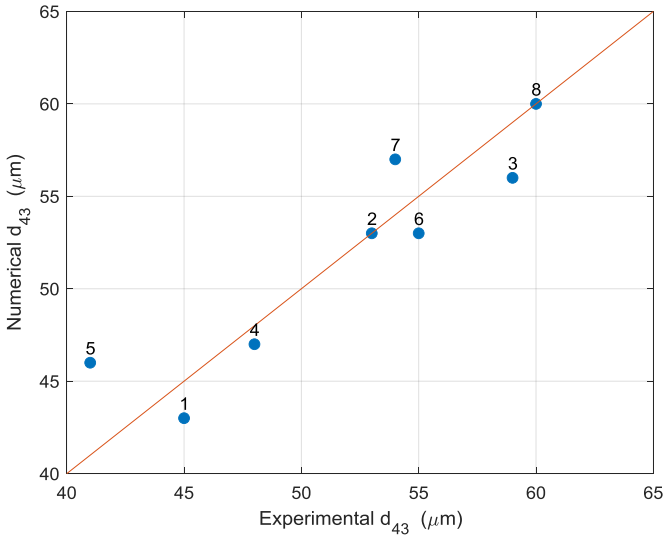

Figure 5. Comparison between experimental and simulated mean crystal sizes for the conditions reported in ~~**Erreur ! Source du renvoi introuvable.**~~Table 1.

4. Conclusions

In this work, a numerical methodology to solve the Population Balance Equation (PBE) including nucleation, size-independent growth and loose agglomeration in a Mixed Suspension Mixed Product Removal (MSMPR) precipitator was developed for the steady state case. It is based on the solution of two coupled PBEs by a discretization method. The PBE formulation takes into account several input streams and no assumption is made about the solid phase entering to the control volume.

The PBE for the crystallites raises in an ordinary differential equation which can be easily solved numerically. Concerning the agglomerates, the PBE is a strongly non-linear and high dimensionality problem. Hence, a fixed point problem is formulated and acrossed-secant acceleration method is included in order to guarantee both convergence and efficiency. No restriction is placed on the location of grid points (quantity or distribution) and a mixed convergence criterion is formulated in order to favour the prediction of the mean size region rather than the furthest portions of the crystal size distribution (CSD). The complete system is solved through the coupling of both PBEs.

The methodology was first validated against analytical solutions. The entire CSD of the crystallites and agglomerates are accurately predicted. The crossed-secant accelerated fixed point improves standard fixed point robustness to solve the agglomeration PBE, especially for high values of the agglomeration characteristic time.

As a second step, the CSD obtained by the developed methodology was compared to a wide range of experimental data. Only the crossed-secant acceleration method achieves agglomeration PBE solution. The mean crystal size and the first seven moments of the CSD are accurately predicted by the numerical method. A slight difference is observed when the entire distribution is compared, which

can be explained by the error propagation induced by the nucleation, growth and agglomeration kinetics models and the inherent experimental uncertainty. The convergence performances are independent of the operating conditions when the acceleration method is included on the PBE solution algorithm for agglomeration. The proposed numerical methodology is then has proven to be efficient and robust. Moreover, the computing performances are really satisfactory and the assumptions made are suitable for future coupling with a multicompartmental model or CFD calculations [31].

Nomenclature

b	Boundaries of the size ranges	m
B	Birth term	$m^{-4}\ s^{-1}$
C	Molar composition	$mol\ m^{-3}$
D	Death term	$m^{-4}\ s^{-1}$
F	Flowrate	$m^{3}\ s^{-1}$
G	Growth rate	$m\ s^{-1}$
I	Ionic force	$mol\ m^{-3}$
I_0, I_1	Modified Bessel functions	-
J	Dimensionless CSD	-
K	Total quantity of nodes	-
L	Crystal size	m
L^*	nuclei size	m
M	Total quantity of streams	-
n	Number-based density function	m^{-4}
N	Total number of particles	m^{-3}
P_s	Solubility product	$mol^{5}\ m^{-15}$
R	Ideal gas constant	$J\ mol^{-1}\ K^{-1}$
r_{Ag}	Agglomeration rate	$m^{-4}\ s^{-1}$
R_N	Nucleation rate	$m^{3}\ s^{-1}$
S	Relative supersaturation	-
t	Time	s
t'	Agglomeration characteristic time	-
V	Reactor volume	m^{3}
v	Crystal volume	m^{3}

Greek symbols

β	Agglomeration kernel	$m^{3}\ s^{-1}$
δ	Dirac delta function	-
$\delta_{p,q}$	Kronecker function	-
ε_a	Absolute tolerance	m^{-3}
ε_r	Relative tolerance	-
η	Weight coefficient	-
λ	Crystal size	M
τ	Mean residence time	S
$\gamma_{\pm}$	Activity coefficient	-
$\dot{\gamma}$	Shear rate	s^{-1}

Index

i	Stream
j	Iteration number
k	Position in the discretization vector
M	Output stream
p,q	Mother particles in agglomeration

Abbreviations

CFD	Computational Fluid Dynamics
CSD	Crystal Size Distribution
MSMPR	Mixed Solution Mixed Product Removal
PBE	Population Balance Equation

Acknowledgments

The authors thank ORANO for its financial support.

References

[1] N. Yazdanpanah et Z. K. Nagy, « The Handbook of Continuous Crystallization », p. 629.
[2] A. S. Myerson, D. Erdemir, et A. Y. Lee, *Handbook of Industrial Crystallization*. Cambridge University Press, 2019. [En ligne]. Disponible sur: https://books.google.fr/books?id=gQVvuwEACAAJ
[3] H. M. Hulburt et S. Katz, « Some problems in particle technology », *Chemical Engineering Science*, vol. 19, n° 8, p. 555- 574, août 1964, doi: 10.1016/0009-2509(64)85047-8.
[4] A. Mersmann, *Crystallization Technology Handbook.* Hoboken: Marcel Dekker Inc., 2001. Consulté le: janv. 30, 2019. [En ligne]. Disponible sur: http://public.eblib.com/choice/publicfullrecord.aspx?p=216050
[5] D. Ramkrishna et M. R. Singh, « Population Balance Modeling: Current Status and Future Prospects », *Annual Review of Chemical and Biomolecular Engineering*, vol. 5, n° 1, p. 123- 146, juin 2014, doi: 10.1146/annurev-chembioeng-060713-040241.
[6] H. M. Omar et S. Rohani, « Crystal Population Balance Formulation and Solution Methods: A Review », *Crystal Growth & Design*, vol. 17, n° 7, p. 4028- 4041, juill. 2017, doi: 10.1021/acs.cgd.7b00645.
[7] T. Wang *et al.*, « Recent progress of continuous crystallization », *Journal of industrial and engineering chemistry*, vol. 54, p. 14- 29, 2017.
[8] J. Kumar, G. Warnecke, M. Peglow, et S. Heinrich, « Comparison of numerical methods for solving population balance equations incorporating aggregation and breakage », *Powder Technology*, vol. 189, n° 2, p. 218- 229, janv. 2009, doi: 10.1016/j.powtec.2008.04.014.
[9] A. F. Blandin, D. Mangin, C. Subero-Couroyer, A. Rivoire, J. P. Klein, et J. M. Bossoutrot, « Modelling of agglomeration in suspension: Application to salicylic acid microparticles », *Powder Technology*, vol. 156, n° 1, p. 19- 33, août 2005, doi: 10.1016/j.powtec.2005.05.049.
[10] Z.-H. Luo, P.-L. Su, X.-Z. You, D.-P. Shi, et J.-C. Wu, « Steady-state particle size distribution modeling of polypropylene produced in tubular loop reactors », *Chemical Engineering Journal*, p. 11, 2009.
[11] M. Jaradat, « Effect of phase dispersion and mass transfer direction on steady state RDC performance using population balance modelling », *Chemical Engineering Journal*, p. 9, 2010.
[12] A. Buffo, « Simplified volume-averaged models for liquid–liquid dispersions_ Correct derivation and comparison with other approaches », *Chemical Engineering Science*, p. 12, 2016.
[13] M. Shiea, A. Buffo, M. Vanni, et D. Marchisio, « Numerical Methods for the Solution of Population Balance Equations Coupled with Computational Fluid Dynamics », *Annu. Rev. Chem.*

Biomol. Eng., vol. 11, n° 1, p. 339‑ 366, juin 2020, doi: 10.1146/annurev-chembioeng-092319-075814.
[14] M. J. Hounslow, « A discretized population balance for continuous systems at steady state », *AIChE Journal*, vol. 36, n° 1, p. 106‑ 116, janv. 1990, doi: 10.1002/aic.690360113.
[15] M. Nicmanis et M. J. Hounslow, « Finite-element methods for steady-state population balance equations », *AIChE Journal*, vol. 44, n° 10, p. 2258‑ 2272, 1998, doi: 10.1002/aic.690441015.
[16] N. Semlali Aouragh Hassani, K. Saidi, et T. Bounahmidi, « Steady state modeling and simulation of an industrial sugar continuous crystallizer », *Computers & Chemical Engineering*, vol. 25, n° 9, p. 1351‑ 1370, sept. 2001, doi: 10.1016/S0098-1354(01)00705-0.
[17] S. Alzyod, M. Attarakih, A. Hasseine, et H.-J. Bart, « Steady state modeling of Kühni liquid extraction column using the Spatially Mixed Sectional Quadrature Method of Moments (SM-SQMOM) », *Chemical Engineering Research and Design*, vol. 117, p. 549‑ 556, janv. 2017, doi: 10.1016/j.cherd.2016.11.013.
[18] S. Lalleman, M. Bertrand, et E. Plasari, « Physical simulation of precipitation of radioactive element oxalates by using the harmless neodymium oxalate for studying the agglomeration phenomena », *Journal of Crystal Growth*, vol. 342, n° 1, p. 42‑ 49, mars 2012, doi: 10.1016/j.jcrysgro.2011.01.079.
[19] M. Bertrand-Andrieu, E. Plasari, et P. Baron, « Determination of Nucleation and Crystal Growth Kinetics in Hostile Environment – Application to the Tetravalent Uranium Oxalate U(C2O4)2. 6H2O », *The Canadian Journal of Chemical Engineering*, vol. 82, n° 5, p. 930‑ 938, mai 2008, doi: 10.1002/cjce.5450820508.
[20] S. Kumar et D. Ramkrishna, « On the solution of population balance equations by discretization—I. A fixed pivot technique », *Chemical Engineering Science*, vol. 51, n° 8, p. 1311‑ 1332, avr. 1996, doi: 10.1016/0009-2509(96)88489-2.
[21] B. Michel, T. Helfer, I. Ramière, et C. Esnoul, « A new numerical methodology for simulation of unstable crack growth in time independent brittle materials », *Engineering Fracture Mechanics*, vol. 188, p. 126‑ 150, févr. 2018, doi: 10.1016/j.engfracmech.2017.08.009.
[22] C. Brezinski et L. Wuytack, *Numerical Analysis: Historical Developments in the 20th Century.* Amsterdam: Elsevier Science, 2014. Consulté le: mai 20, 2021. [En ligne]. Disponible sur: http://qut.eblib.com.au/patron/FullRecord.aspx?p=1191024
[23] C. Brezinski, « Convergence acceleration during the 20th century », *Journal of Computational and Applied Mathematics*, p. 21, 2000.
[24] D. G. Anderson, « Iterative Procedures for Nonlinear Integral Equations », p. 14.
[25] I. Ramière et T. Helfer, « Iterative residual-based vector methods to accelerate fixed point iterations », *Computers & Mathematics with Applications*, vol. 70, n° 9, p. 2210‑ 2226, nov. 2015, doi: 10.1016/j.camwa.2015.08.025.
[26] C. Bresinski, *Accélération de la convergence en analyse numérique*. New York: Springer-Verlag, 1977.
[27] A. D. Randolph et M. A. Larson, « Transient and steady state size distributions in continuous mixed suspension crystallizers », *AIChE Journal*, vol. 8, n° 5, p. 639‑ 645, 1962.
[28] A. D. Randolph et M. A. Larson, *Theory of particulate processes: analysis and techniques of continuous crystallization*. New York: Academic Press, 1971.
[29] L. A. Bromley, « Thermodynamic properties of strong electrolytes in aqueous solutions », *AIChE J.*, vol. 19, n° 2, p. 313‑ 320, mars 1973, doi: 10.1002/aic.690190216.
[30] S. Lalleman, M. Bertrand, E. Plasari, C. Sorel, et P. Moisy, « Determination of the Bromley contributions to estimate the activity coefficient of neodymium electrolytes », *Chemical Engineering Science*, vol. 77, p. 189‑ 195, juill. 2012, doi: 10.1016/j.ces.2012.02.011.
[31] E. Saikali *et al.*, « Validation of the hydrodynamics in a turbulent un-baffled stirred tank: A necessity for vortex-reactor precipitation studies », *Chemical Engineering Science*, vol. 214, p. 115426, mars 2020, doi: 10.1016/j.ces.2019.115426.

Appendix 1. Comparison of acceleration methods and influence of the initial vector. (Study case)

Method		$\boldsymbol{N}^0 = N_{in}$		$\boldsymbol{N}^0 = 0$		$\boldsymbol{N}^0 = \frac{N_{in}}{t'}$
		$t' = 1$	$t' = 10^3$	$t' = 1$	$t' = 10^3$	$t' = 10^3$
Fixed point iterations		55 iterations	Diverges	56 iterations	Diverges	Diverges
K-dimensional scalar secant method		42 iterations	Very slow convergence	43 iterations	Very slow convergence	Very slow convergence
Vector acceleration	Crossed secant	18 iterations	Very slow convergence	20 iterations	156 iterations	154 iterations
	Alternate secant	23 iterations	Diverges	27 iterations	Diverges	Diverges

Table 2. Numerical performances of the acceleration methods tested to solve the agglomeration fixed point problem over different initialization vectors ($\beta = 10^{-16}$ and $N_0 = 10^{16}$).

Appendix 2. Convergence performances with respect to the number of discretization points and agglomeration characteristic time. (Theoretical case)

	40 points		100 points		200 points	
t'=0.25	7 iterations	< 1s	7 iterations	< 1s	7 iterations	3 s
t'=1	18 iterations	< 1s	18 iterations	1 s	18 iterations	9 s
t'=1.5	Diverges	-	Diverges	-	Diverges	-

Table 3. Numerical performances of the standard fixed point iterations to solve the agglomerates PBE ($\beta = 1$ and $N_0 = 1$).

	40 points		100 points		200 points	
t'=0.25	7 iterations	< 1s	7 iterations	< 1s	7 iterations	3 s
t'=1	10 iterations	< 1s	12 iterations	1 s	12 iterations	8 s
t'=1.5	12 iterations	< 1s	13 iterations	1 s	14 iterations	9 s
t'=10	20 iterations	< 1s	24 iterations	2 s	25 iterations	13 s
t'=100	35 iterations	< 1s	44 iterations	3 s	47 iterations	25 s
t'=1000	49 iterations	< 1s	65 iterations	4.5 s	73 iterations	40 s

Table 4. Numerical performances of the accelerated fixed point algorithm (crossed-secant method) to solve the agglomerates PBE ($\beta = 1$ and $N_0 = 1$).